Interpretation of Fluctuation Spectra in Lipid Bilayer Simulations

Erik G. Brandt,[†] Anthony R. Braun,[‡] Jonathan N. Sachs,[‡] John F. Nagle,[§] and Olle Edholm[†*]
[†]Department of Theoretical Physics, Royal Institute of Technology, Stockholm, Sweden; [‡]Department of Biomedical Engineering, University of Minnesota, Minneapolis, Minnesota; and [§]Department of Physics, Carnegie Mellon University, Pittsburgh, Pennsylvania

ABSTRACT Atomic resolution and coarse-grained simulations of dimyristoylphosphatidylcholine lipid bilayers were analyzed for fluctuations perpendicular to the bilayer using a completely Fourier-based method. We find that the fluctuation spectrum of motions perpendicular to the bilayer can be decomposed into just two parts: 1), a pure undulation spectrum proportional to q^{-4} that dominates in the small-q regime; and 2), a molecular density structure factor contribution that dominates in the large-q regime. There is no need for a term proportional to q^{-2} that has been postulated for protrusion fluctuations and that appeared to have been necessary to fit the spectrum for intermediate q. We suggest that earlier reports of such a term were due to the artifact of binning and smoothing in real space before obtaining the Fourier spectrum. The observability of an intermediate protrusion regime from the fluctuation spectrum is discussed based on measured and calculated material constants.

INTRODUCTION

Biological membranes undergo significant structural fluctuations that are thermally excited at physiological temperatures. This has been studied experimentally with a number of different techniques (1–6). The fluctuations include undulations, peristaltic thickness fluctuations, and more local protrusion modes. These motions occur in living cells and are important for the functioning of the membranes. The equilibrium properties of undulating lipid bilayers have long been successfully modeled using Helfrich-type continuum models (7). The essential prediction is that the undulations have a fluctuation spectrum, often called the undulation structure factor (mean-square Fourier component of the membrane surface) that is proportional to the inverse fourth power of the wave vector, and thus diverges at small wave vectors. This power-law behavior can be verified in more or less direct ways with various experimental techniques, most directly by Fourier analysis of images of giant vesicles (8). Thus, a bending modulus ranging from a few up to ~100 k_BT can be extracted depending on membrane and lipid type (9).

This article is one out of two in which detailed analysis of these fluctuations is performed based on extensive molecular dynamics simulations. In the second article (10), the aim is to calculate an (electron) density across the membrane to compare to experiment. Undulations in large-scale simulations blur the simulated electron density and must therefore be removed. However, local molecular motions and protrusions are contained in the experimental data and must therefore not be removed from the simulations. In this article the main focus is to separate undulations from the other fluctuations. In addition to the practical importance of correcting simulations to be suitable for comparison to experiment performed in Braun et al. (10), this separation involves the fundamental issue of characterizing the contributions of different kinds of fluctuations in the overall fluctuation spectrum.

The theory and experiments are all pertinent on length-scales that are much larger than typical intermolecular distances in the bilayer. During the last 10 years, membrane fluctuations have been studied from the other end of the length-scale using molecular simulations (11,12). Wavelengths up to ~20 nm (corresponding to wave vectors $2\pi/\lambda$ down to ~0.3 nm^{-1}) are long enough to reach the validity regime of continuum theories, typically ~1 nm^{-1}. This requires large simulations, including those of the order of 1000 lipids—which is 10^5 atoms in the atomistic case, fewer with coarse-graining, that need to be run for a long time (10–100 ns) for the large wavelength modes to develop.

The speed of present supercomputers makes it possible to extend system sizes by 2–3 orders of magnitude, which would bring us one-order-of-magnitude smaller wave vectors and give a larger q-regime over which continuum theories should be valid. This is, however, hampered by the time it takes to develop and equilibrate the large wavelength modes. Theory (see, e.g., the review by Edholm (13)) indicates that equilibration times scale with wavelength-cubed, although recent simulations show that the power appears to be somewhat smaller (14). Doing atomistic simulations with considerably greater than 1000 lipids would be a possible direction to go to extend the power-law regime to smaller q. In this article, we supplement 1024-lipid atomistic simulations by taking advantage of the faster dynamics of a coarse-grained simulation with 8192 lipids in total, to extend q down to 0.1 nm^{-1}. Further extension to smaller q is not necessary for the focus of this article.

The focus of this work is on the spectrum for q larger than 1 nm^{-1} where one begins to leave the realm of continuum theory. The early work (12,15) seemed to indicate that the q^{-4} undulation regime crossed over to an earlier proposed protrusion regime with a q^{-2} spectrum (16,17). At still

Submitted December 15, 2010, and accepted for publication March 2, 2011.

*Correspondence: oed@kth.se

Editor: Scott Feller.

0006-3495/11/05/2104/8 $2.00

doi: 10.1016/j.bpj.2011.03.010

larger q, it was assumed that just noise remained or that the spectrum approached zero. We now suggest that an accurate analysis of the large-q regime was hampered by the use of a finite grid and smoothing functions in real space. We have therefore adopted a completely Fourier-based calculation of the fluctuation spectrum.

This method has previously been applied to capillary waves on a liquid surface (18,19) and to coarse-grained lipid bilayers (20–23) with the result that there is an increase in the structure factor in the large-q regime before it reaches a constant value. We will discuss this in more detail and show that the large-q regime of the spectrum can be directly related to the two-dimensional density structure factor. We will further discuss to what extent protrusions have an impact on the fluctuation spectra of lipid bilayers. For our simulations, we find that in the intermediate q regime, where protrusions should dominate the undulations, the molecular structure reflected in the density structure factor instead outweighs possible protrusions. Thus, for the atomistic and the coarse-grained lipid models studied here, we do not find any room for a protrusion regime when interpreting the spectra.

CONTINUUM THEORY

The simplest, Helfrich-type continuum model (7) for lipid bilayer undulations describes the bilayer as a single mathematical surface $u(x, y)$, illustrated in Fig. 1. The Hamiltonian then assumes that flat surfaces $u(x, y) = u_0$ have minimum energy and that there is a local energetic cost to deform this surface. When studying thermally excited energy fluctuations, the Hamiltonian may be expanded with the lowest-order terms being

$$H\{u(x,\ y)\} \ = \frac{1}{2}\iint \left[k_c|\nabla^2 u(x,\ y)|^2 + \gamma|\nabla u(x,\ y)|^2\right] \mathrm{d}x\mathrm{d}y. \qquad (1)$$

(Note that linear terms are absent for a symmetric bilayer.) The first term is a bending term, with the constant k_c being the bending modulus. The second term is a surface tension term, which is proportional to the excess surface area, with γ being the surface tension coefficient. The analysis is most conveniently performed by Fourier expansion

$$u(\mathbf{r}) \ = \sum_{\mathbf{q}} u\ (\mathbf{q})\ e^{i\mathbf{q}\cdot\mathbf{r}}, \qquad (2)$$

with $\mathbf{r} = (x, y)$ being a two-dimensional real space vector and $\mathbf{q} = (q_x, q_y)$ being the two-dimensional reciprocal space vector. Then, the quadratic Hamiltonian of Eq. 1 ensures that the Fourier modes decouple and equipartition can be utilized to give the fluctuation spectrum

$$S_u(q) \equiv N\langle|u(q)|^2\rangle \ = \frac{k_\mathrm{B}T}{a(k_c q^4 + \gamma q^2)} = \{\gamma \ = 0\} = \frac{k_\mathrm{B}T}{ak_c q^4}, \qquad (3)$$

with $a = A/N$ being the projected area per lipid (N is the number of lipids per monolayer) in the $(x, y, z = 0)$-plane. The angular brackets denote an ensemble average.

Unlike fluids with a free surface in a fixed container, the projected area of a bilayer is free to fluctuate and to adjust its average by changing the average thickness to attain the area that minimizes the free energy; this corresponds to surface tension $\gamma = 0$. A nonzero surface tension in Eq. 3 would affect the intensity of the small-q modes (large wavelengths), which would become proportional to q^{-2} instead of q^{-4} for

$$q \ll \sqrt{\gamma/k_c}.$$

To completely eliminate the q^{-4} regime, which typically extends up to 1 nm^{-1} (shown later) a surface tension of 0.1 N/m would be required assuming a k_c of 10^{-19} J. The entire study addressed in this article has, however, been performed at vanishing surface tension, using a barostat that yields a time-averaged surface tension of ~10^{-5} N/m, while mimicking the large instantaneous fluctuations of ~0.1 N/m, associated with small-system simulations. Thus, the q^{-4} behavior of Eq. 3 will be attained in the simulations.

As shown in Fig. 1, undulations $u(x, y)$ are due to correlated fluctuations of the two monolayer surfaces. Anti-correlated fluctuations of the monolayer surfaces show up as local thickness fluctuations, $h(x, y)$. Assuming a volume-conserving (i.e., peristaltic) approximation, $h(x, y)$is anti-correlated to the area fluctuations and can be described by a similar continuum theory, but with different q dependence, as the undulations (12).

In addition, local protrusion modes have been suggested. They can be viewed as uncorrelated fluctuations of the two monolayer surfaces, subject to a microscopic protrusion tension, γ_p. These modes have been supposed to equipartition separately from the undulations, which results in a q^{-2} spectrum. This gives the intensity of the full Fourier modes of a system at zero macroscopic surface tension as (16,17)

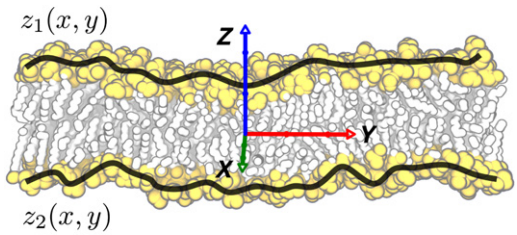

$$u(x,y) = \frac{1}{2}(z_1(x,y) + z_2(x,y))$$

$$h(x,y) = \frac{1}{2}(z_1(x,y) - z_2(x,y))$$

FIGURE 1 Schematic drawing illustrating the monolayer surfaces and the definitions of the bilayer undulations, $u(x,y)$, and the thickness, $h(x,y)$.

$$S_u(q) = \frac{k_B T}{a}\left[\frac{1}{k_c q^4} + \frac{1}{\gamma_p q^2}\right]. \quad (4)$$

Alternatively, a q^{-2} term has recently been attributed to molecular tilt (24). A more recent theory for protrusions adds a constant k_p in the denominator of the last term which gives a constant, finite small-q limit (25) for the protrusion term. This variation will be discussed later. In the original theory, i.e., as described by Eq. 4, undulations dominate at small q. Values of q larger than

$$q_p = \sqrt{\gamma_p / k_c} \quad (5)$$

would be needed for protrusions to dominate over undulations. With $k_c = 10^{-19}$ J and $\gamma_p = 0.01$–0.20 N/m, we get $q_p = 0.3$–1.4 nm^{-1}. With $\langle |u(q)|^2 \rangle$ calculated from simulations and plotted versus q, a crossover behavior from q^{-4} to q^{-2} behavior has often been reported before the intensities have reached a constant noisy level at large q (11,12,15,25). This has been attributed to protrusions with reported values of γ_p in the range given above. We emphasize, however, that this analysis usually has been done using a grid in real space and sometimes smoothing of the functions using spline methods. Thus, it is not surprising that a smooth transition to the noise level in q space was obtained, which at limited numerical resolution was interpreted as a q^{-2} regime.

We will here instead do the analysis directly in Fourier space based on the instantaneous atomic positions, which allows us to reach very large q. This will show that $S_u(q)$ approaches a renormalized area number density structure factor that essentially is the Fourier transform of the two-dimensional pair correlation function. Subtracting this well identified contribution, we may focus on the remaining spectrum, without corruption from artifacts of real space filtering.

SIMULATION DETAILS

Two different force fields were used to represent different (but overlapping) levels of detail of 1,2-dimyristoyl-*sn*-glycero-3-phosphocholine (DMPC) and water molecules. The first was the united-atom (UA) force field of Berger et al. (26), which is atomistic except for nonpolar hydrogens being included into single beads for CH, CH_2, and CH_3 groups. The hydration level used was 23 waters per lipid, modeled by the simple-point-charge water model (27). The Berger force field reproduces important structural (12) and dynamical quantities (28,29) of phospholipid bilayers well. To enable simulations of larger systems for longer times, the coarse-grained (CG) MARTINI force field (30,31) was used, which maps roughly four nonhydrogen atoms to one interaction center; this reduces the 14 hydrocarbon groups in the fatty acid chain of DMPC to either three or four particle beads. We chose three beads. Waters are incorporated in the MARTINI force field as van der Waals spheres, each representing four water molecules.

Following Brandt and Edholm (14), a lipid bilayer with 1024 lipids was constructed starting from the atomic coordinates of the unit cell of crystal structure DMPC (32). The coarse-grained system was constructed from the atomistic system and replicated to contain 8192 lipids.

Molecular dynamics simulations were performed with the GROMACS 4 program, using a leap-frog algorithm to integrate the equations of motion (33). To determine when a simulation was equilibrated, potential energy and area per lipid were monitored. In addition, the Fourier intensities at the lowest wave vectors ($q < 1$ nm^{-1}) were averaged over successive 10-ns intervals. When these average intensities ceased changing, the system was considered to be in equilibrium and production simulations were then run for an additional 1–2 μs. All simulations were run in parallel on a supercomputer cluster with two Quad-Core CPUs per node, with the systems prepared in the isothermal-isobaric (NPT) ensemble at constant temperature and pressure, corresponding to 300 K and 1 bar, respectively. The resulting area per lipid was 0.605 ± 0.004 nm^2 for the atomistic system and slightly smaller, 0.587 ± 0.002 nm^2 for the coarse-grained system. This should be compared to the experimental value of 0.606 ± 0.005 nm^2 (34).

The following parameters were specific to the UA simulations. The time integration was performed with a 4-fs time step, with atom bonds constrained by the P-LINCS algorithm (35). A neighbor list, recalculated every 10th step, was used up to 1.0 nm and a cutoff at 1.0 nm was applied for nonbonded interactions. The van der Waals interactions were simply truncated at this distance, whereas electrostatic interactions were calculated directly in real space up to the cutoff, and in Fourier space beyond, with Ewald summation using particle-mesh Ewald (36,37). The grid spacing in the particle-mesh Ewald algorithm was set to 0.12 nm. A Nosé-Hoover thermostat (38,39) with a time constant of 0.5 ps was used to control the ensemble temperature, while an analog Parrinello-Rahman barostat (40,41) with a time constant of 50 ps was used to keep the pressure fixed. The lipids and the water were coupled to independent thermostats to avoid unwanted heating/cooling artifacts. For the barostat, the lateral box dimensions were coupled independently in the normal and lateral dimensions to the pressure 1 bar, to give a tensionless bilayer.

For the CG simulations, essentially the original parameters (31) were used. The integration time step was 40 fs. Nonbonded interactions were included by Coulomb and Lennard-Jones potentials, with energies and forces shifted to smoothly approach zero at the cutoff. The Lennard-Jones interactions were reduced beginning at 0.9 nm to vanish at 1.2 nm while the Coulomb interactions were reduced continuously in the entire range up to 1.2 nm. Explicit charge screening was included by scaling the electrostatic

interactions with a relative dielectric constant $\varepsilon_r = 15$. A neighbor list with a range of 1.2 nm was set up and regenerated every 10th simulation step, whereas the ensemble temperature and pressure was controlled at the same state point (300 K and 1 bar) and in the same way as for the UA simulations but with different time constants, 2.5 ps for the thermostat and 250 ps for the barostat.

ANALYSIS OF THE SIMULATIONS

In the analysis, the lipid bilayer is represented by the two monolayer surfaces $z_1(x,y)$ and $z_2(x,y)$ ($z_1 > z_2$) (Fig. 1). The undulating surface is then described by

$$u(x,\ y)\ =\ \frac{1}{2}(z_1(x,\ y) + z_2(x,\ y)), \tag{6}$$

whereas half the local membrane thickness is given as

$$h(x,\ y)\ =\ \frac{1}{2}(z_1(x,\ y) - z_2(x,\ y)). \tag{7}$$

We chose the phosphate atoms of the headgroups to represent the surfaces. Other choices are shown in the next article of Braun et al. (10); they make no essential differences in this article. The local area number density is defined as an average of the phosphate number densities projected onto the lateral plane,

$$\rho(x,\ y)\ =\ \frac{1}{2}\Big(\rho_{1_\parallel}(x,\ y) + \rho_{2_\parallel}(x,\ y)\Big). \tag{8}$$

A Fourier expansion of the monolayer surfaces $j = 1, 2$ is introduced as

$$\begin{aligned} z_j(\mathbf{r})\ &=\ \sum_{\mathbf{q}} z_j(\mathbf{q})e^{i\mathbf{q}\cdot\mathbf{r}} \quad \text{with} \\ z_j(\mathbf{q})\ &=\ \frac{1}{A}\iint z_j(\mathbf{r})e^{-i\mathbf{q}\cdot\mathbf{r}}\mathrm{d}^2\mathbf{r} \end{aligned} \tag{9}$$

with $A = L_xL_y$ being the projected area of the bilayer. The in-plane coordinates are $\mathbf{r} = (x, y)$, and the sum in Eq. 9 is taken over all wave vectors $\mathbf{q} = 2\pi(n/L_x,\ m/L_y)$ with $n, m = 0,\ \pm1,\ \pm2,\ \pm3\ldots$. Using the instantaneous atomic positions ($\mathbf{r}_{jk}$, z_{jk}), we recenter the height of the bilayer in each frame so that

$$\sum_{j,\ k} z_{jk}\ =\ 0.$$

The Fourier coefficients of the bilayer surface are then

$$u(\mathbf{q})\ =\ \frac{1}{2N}\sum_{k=1}^{N}\left[z_{1k}e^{-i\mathbf{q}\cdot\mathbf{r}_{1k}} + z_{2k}e^{-i\mathbf{q}\cdot\mathbf{r}_{2k}}\right] \tag{10}$$

and the Fourier coefficients of the thickness fluctuations are

$$h(\mathbf{q})\ =\ \frac{1}{2N}\sum_{k=1}^{N}\left[z_{1k}e^{-i\mathbf{q}\cdot\mathbf{r}_{1k}} - z_{2k}e^{-i\mathbf{q}\cdot\mathbf{r}_{2k}}\right]. \tag{11}$$

The Fourier components of the (projected) area number density are written as

$$\rho(\mathbf{q})\ =\ \frac{1}{2aN}\sum_{k=1}^{N}\left[e^{-i\mathbf{q}\cdot\mathbf{r}_{1k}} + e^{-i\mathbf{q}\cdot\mathbf{r}_{2k}}\right], \tag{12}$$

with N being the number of lipids in each monolayer.

The fact that $u(\mathbf{r})$, $h(\mathbf{r})$, and $\rho(\mathbf{r})$ are real functions guarantees that their Fourier coefficients fulfill the relations $u(\mathbf{q}) = u^*(-\mathbf{q})$, $h(\mathbf{q}) = h^*(-\mathbf{q})$, and $\rho(\mathbf{q}) = \rho^*(-\mathbf{q})$. Imposing periodic boundary conditions discretizes the wave vectors and establishes a small-q cutoff $2\pi/L_{\max}$, where $L_{\max}$ is the largest box length. In the UA 1024-lipid simulation, $L_{\max} = 17$ nm, giving a cutoff wave vector at 0.36 nm^{-1}; in the CG 8192-lipid simulation, $L_{\max} = 49$ nm, with a corresponding cutoff at 0.13 nm^{-1}.

The fluctuation spectra for u and h are defined as

$$S_u(q)\ =\ N\left\langle\left|u(q)\right|^2\right\rangle \text{ and } S_h(q)\ =\ N|h(q)|^2, \tag{13}$$

with the angular brackets indicating averages over simulation time. (These fluctuation spectra are often called structure factors, but one should not confuse them with structure factors obtained from diffraction experiments which are related to the average unit cell structure.) The inclusion of the N normalization factor in these definitions makes these spectra largely independent of system size, which is convenient for comparisons. Importantly, both S_u and S_h have the same large-q limit (see Sections S1 and S2 in the Supporting Material for the derivation),

$$\frac{1}{2}\left[\left\langle h^2\right\rangle + \left\langle u^2\right\rangle\right], \tag{14}$$

with $\langle h^2\rangle$ and $\langle u^2\rangle$ being space- and time-averages. For the number density structure factor, we choose a somewhat unconventional normalization,

$$S_\rho(q)\ =\ Na^2\left[\left\langle h^2\right\rangle + \left\langle u^2\right\rangle\right]\left\langle\left|\rho(q)\right|^2\right\rangle, \tag{15}$$

that gives the same large-q limit as $S_u(q)$ and $S_h(q)$. (The conventional limit in liquid-state theory, for example, from Hansen and McDonald (42), is 1.) The relevant fluctuation spectra are calculated directly in Fourier space from the stored coordinates using Eqs. 10–12, averaging over circles of radii

$$q\ =\ |\mathbf{q}|\ =\ \sqrt{q_x^2 + q_y^2},$$

with bin-width $\Delta q = 0.05$ nm^{-1}.

RESULTS

Fig. 2 shows $S_\rho(q)$. In the large q limit, it approaches the value given by Eq. 14 as expected from the normalization in Eq. 15 and by the vanishing in-plane correlations at large q (small r). The limiting value at small q is given by a compressibility relation of similar type as that of three-dimensional bulk fluids (42). In two dimensions, this reads

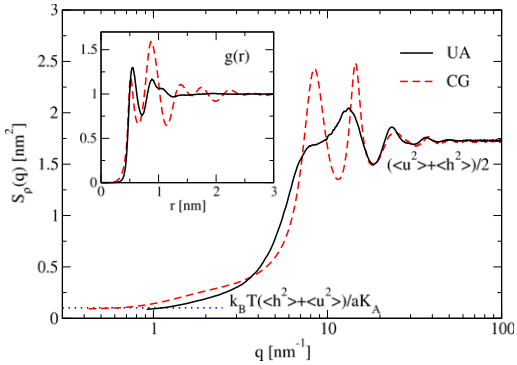

FIGURE 2 Static number density structure factor, $S_\rho(q)$, for the UA and CG systems (normalized as described in the text) shown versus q. At small q the structure factor reaches the limiting value, $k_BT(\langle u^2\rangle + \langle h^2\rangle)/aK_A$, given by the compressibility equation (Eq. 16). This value is indicated (*dotted line*) for $K_A = 0.234$ N/m. For large q, it approaches $(\langle u_2\rangle + \langle h^2\rangle)/2$ (derived in Section S2 in the Supporting Material). (*Inset*) The corresponding radial distribution function $g(r)$ (the inverse two-dimensional Fourier transform of $\langle|\rho(q)|^2\rangle$). The value of $g(r)$ approaches 1 at large distances in these units, which corresponds to the bulk number density. The function $g(r)$ was calculated by inverse numerical Fourier transform of $\langle|\rho(q)|^2\rangle$ and also by direct calculation in real space; the results were very similar.

(see Section S3 in the Supporting Material for the derivation)

$$S_\rho(0) = \frac{k_BT}{aK_A}\left[\langle u^2\rangle + \langle h^2\rangle\right]. \quad (16)$$

The experimental area compressibility, $K_A = 0.234$ N/m for DMPC (5), gives the small-q limit 0.10 nm^2 for the density structure factor. This is slightly larger than the value 0.07–0.08 that can be read off from the logarithmic plot in Fig. 3. The oscillations in $S_\rho(q)$ for intermediate and large q are inherent to the molecular structure of fluid phases, the unnormalized S_ρ being in fact the inverse Fourier transform of the pair correlation function $g(r)$ shown in the inset of Fig. 2.

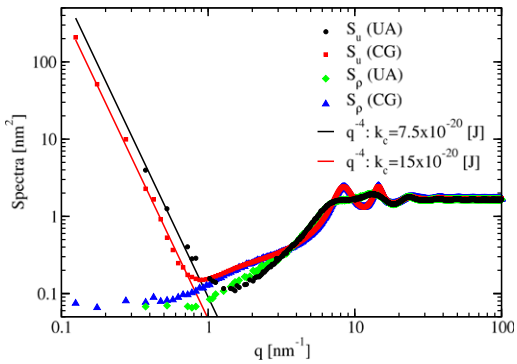

FIGURE 3 Undulation spectra $S_u(q)$ for the UA and CG systems versus wave vector q. Fits are shown to the small-q data of Eq. 3, with $k_c = 7.5 \times 10^{-20}$ J for the UA system and 15×10^{-20} J for the CG system. The number density structure factors $S_\rho(q)$ are plotted to illustrate the agreement in the intermediate-q and large-q regimes.

Fig. 3 shows $S_u(q)$ for the UA system (containing $2N = 1024$ lipids) and the CG system ($2N = 8192$ lipids). $S_u(q)$ is well fit by the predicted q^{-4} lines in the double logarithmic plot up to ~0.7 nm^{-1}. After passing through minima at ~1 nm^{-1}, $S_u(q)$ follows closely to $S_\rho(q)$, with the same intermediate oscillations and theoretical large limit value, $(\langle u^2\rangle + \langle h^2\rangle)/2$. There is a slight difference between the large-q limits of the UA and CG systems of ~2%, due to the difference in area per lipid and membrane thickness and the inclusion of larger undulations in the larger coarse-grained system.

The close agreement between $S_u(q)$ and $S_\rho(q)$ in Fig. 3 at large q is emphasized in Fig. 4, *a* and *b*, which shows a corrected undulation structure factor in a logarithmic and a linear plot, obtained by subtracting the density structure factor according to $S_u(q) - S_\rho(q)$. This quantity looks noisy in a logarithmic plot at larger q because we have subtracted two nearly equal numbers. The noise level can be reduced by averaging but there is clearly a small systematic residual left in the interval $2 < q < 20$ nm^{-1}. However, this has neither the shape nor the amplitude expected from protrusions. We suggest that this residual is due to the density structure factor having been calculated on a planar projected surface, not on the undulating membrane. In any case, by removing the imprint of the molecular structure, the data based on the direct Fourier space analysis does

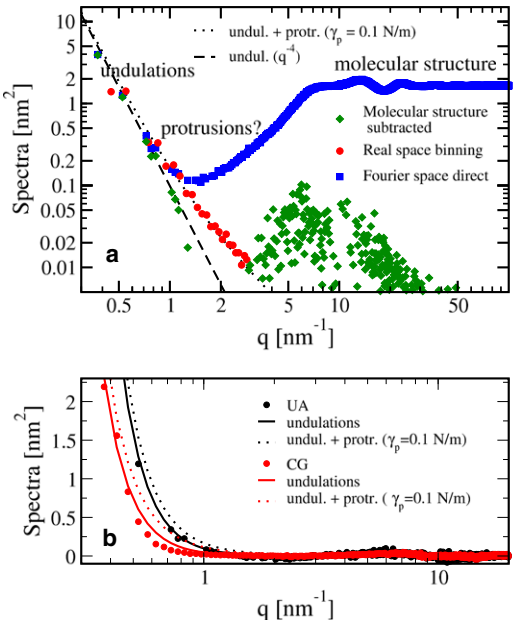

FIGURE 4 (*a*) Data for the UA model. The full $S_u(q)$ spectrum (*squares*) and our suggested undulation spectrum $S_u(q) - S_\rho(q)$ (*diamonds*); the latter is fitted to the theoretical q^{-4} line (Eq. 3). Also shown to illustrate our nonpreferred spectrum is $S_u(q)$ (*circles*) obtained by binning in real space, fitted to Eq. 4 with $\gamma_p = 0.1$ N/m. (*b*) The undulation spectra of the UA and CG models with density structure factor subtracted. The scale is linear for the spectra and logarithmic for q. (*Solid lines*) Fits to q^{-4} lines. (*Dotted line*) Effect of adding a protrusion tension.

now fit a q^{-4} line up to even larger values of q (2–3 nm^{-1}), leaving very little room for inclusion of protrusions with any realistic value of the protrusion tension γ_p.

In contrast, data obtained by binning in real space can be quite well fitted by including a protrusion tension of 0.1 N/m, as shown in Fig. 4 *a*. We used a bin-width of 1.5 nm to obtain at least one lipid per grid point but a finer grid can be used if combined with spline methods. Fig. 5 shows that this gives smooth surfaces for even larger q. The data may now be fitted using the same protrusion tension, γ_p, up to larger q values, but the Fourier coefficients obtained in this way eventually fall off even faster than q^{-4}.

The bending modulus obtained by numerical fits of Eq. 3 to the corrected UA fluctuation spectrum, $S_u(q) - S_\rho(q)$, is 7.5×10^{-20} J. This agrees well with the value 6.5×10^{-20} J obtained from a finite-size scaling analysis performed for the same force field (43), and with the experimental result 6.9×10^{-20} J (34) for DMPC. For the CG model, our value is $k_c = 15 \times 10^{-20}$ J, considerably larger than the value 4×10^{-20} J obtained after binning in real space in the original analysis (30). However, den Otter and Shkulipa (44) reported the value 8×10^{-20} J for the same (MARTINI) force field at a higher temperature ($T =$ 323 K), whereas finite-size scaling as employed in Waheed and Edholm (43) gave 16.7×10^{-20} J (45).

The reason for the pronounced minimum in $S_u(q)$ in Fig. 4 *a* (Fourier space direct data points) is that there is little overlap between the undulation and molecular structure contributions to the spectrum. As q decreases, the $S_\rho(q)$ contribution has already dropped near its small-q limit given by Eq. 16, before $S_u(q) - S_\rho(q)$ takes on appreciable values.

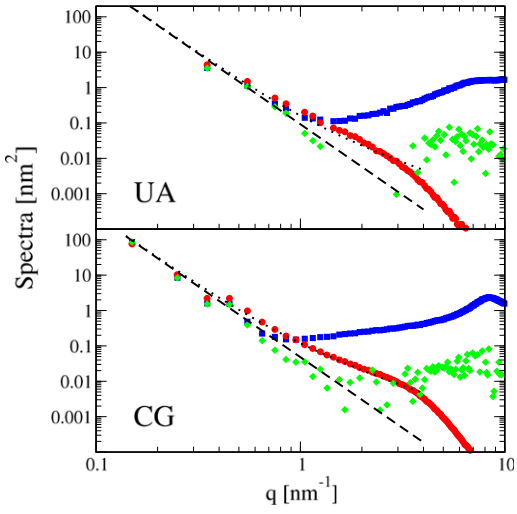

FIGURE 5 Fluctuation spectra $S_u(q)$ (*squares*) and $S_u(q) - S_\rho(q)$ (*diamonds*) in the UA (*top*) and CG (*bottom*) models calculated with the direct Fourier method, compared to $S_u(q)$ (*circles*) calculated with spline interpolation. The direct Fourier method follows a straight q^{-4} line (Eq. 3, *dashed*) whereas the interpolation method introduces an artificial smoothing that gives rise to a q^{-2} broadening (Eq. 4, *dotted*) of the intermediate spectrum q values.

A good approximation to the value q_0 where $S_u(q)$ is a minimum is obtained by equating the undulation contribution $S_u(q) - S_\rho(q)$ to the value of $S_\rho(q)$ in the small-q limit obtained from Eq. 16, according to

$$\frac{k_B T}{a k_c q_0^4} = \left[\langle u^2 \rangle + \langle h^2 \rangle\right] \frac{k_B T}{a K_A}. \tag{17}$$

Although $\langle u^2 \rangle$ is unbounded for an infinite membrane, even the largest simulations have $\langle u^2 \rangle$ equal to just 0.14 nm^2, which is more than an order-of-magnitude less than $\langle h^2 \rangle$ (3.24 nm^2) and may thus be safely neglected. (Recall that the thickness h fluctuates around a nonzero average value, so $\langle h^2 \rangle$ must be as large as $\langle h \rangle^2$.) This gives

$$q_0 = \left(\frac{K_A}{k_c \langle h^2 \rangle}\right)^{1/4}. \tag{18}$$

With material constants from our UA simulations, $\langle h \rangle =$ 1.78 nm, $k_c = 7 \times 10^{-20}$ J, and $K_A = 0.38$ N/m, we obtain $q_0 = 1.15$ nm^{-1}. This is similar to the experimental values for DMPC (5,34), $\langle h \rangle = 1.765$ nm, $k_c = 6.9 \times 10^{-20}$ J, and $K_A = 0.234$ N/m, which yield $q_0 = 1.0$ nm^{-1}. We further note that q_0 is rather insensitive to the values of K_A and k_c due to the small exponent, 1/4. In the following article of Braun et al. (10), we will be interested in obtaining a pure continuum undulation surface for each frame in the simulation. This will be accomplished by filtering out large-q nonundulatory modes. That article shows that such a filter should begin close to q_0 as defined in Eq. 18 to eliminate most of the tracks of the molecular structure, large-q noise, and possible protrusions.

DISCUSSION

A complete model for the out-of-plane fluctuation power spectrum $S_u(q)$ would contain three additive terms,

$$S_u(q) = \frac{k_B T}{a k_c q^4} + \frac{k_B T}{a\left(\gamma_p q^2 + k_p\right)} + S_\rho(q), \tag{19}$$

where the first term, originating from undulations, dominates for small q whereas the last term, originating from in-plane molecular structure fluctuations, dominates at large q. Protrusions, corresponding to the middle term, would therefore have to be seen in an intermediate q regime. Fig. 4 suggests that the middle term is small in the Fourier-based analysis of our simulations. We now wish to discuss under what conditions protrusions might be observable in simulated $S_u(q)$.

Let us begin by considering the traditional theory for which k_p in Eq. 19 is taken to be zero. Protrusions would then be dominated by undulations in $S_u(q)$ for q less than

$$q_{\min} = \sqrt{\gamma_p / k_c}\,.$$

To determine q_{max} at which protrusions would be dominated by in-plane molecular structure fluctuations, first recall that the small-q limit of $S_\rho(q)$ from Eq. 16, assuming that $\langle u^2 \rangle$ can be neglected compared to $\langle h^2 \rangle$, is

$$S_\rho(0) = \frac{k_B T \langle h^2 \rangle}{a K_A}, \tag{20}$$

which is approached from above as q is decreased. Therefore, q_{max} is bounded from above by

$$\sqrt{K_A / (\gamma_p \langle h^2 \rangle)}.$$

To obtain a regime in which protrusions dominate over both undulations and molecular structure contributions, it is required that q_{max} be larger than q_{min}. The criterion for this becomes

$$\gamma_p < \gamma_0 = \sqrt{\frac{k_c K_A}{\langle h^2 \rangle}}, \tag{21}$$

with the experimental numbers inserted for DMPC, $\gamma_0 = 0.07$ N/m. Although the values for γ_p suggested in the literature were obtained using real space methods, which we believe make γ_p too large, even the literature range from 0.03 to 0.18 N/m (11,12,15,25) suggests that a protrusion-dominated regime is either nonexistent or quite small. Of course, it would not be necessary to have a protrusion-dominated regime if the accuracy were sufficient to subtract the first and third terms from $S_u(q)$ to verify the form of the protrusion term and evaluate its parameters. That seems unlikely from Figs. 4 and 5, which show that subtraction of S_ρ leaves an undulation term and some large-q noise that does not have the functional form expected from protrusions.

The same questions may also be asked for nonzero k_p in Eq. 19. The protrusion term then has a crossover from being proportional to $1/(\gamma_p q^2)$ into being proportional to $1/k_p$ when q becomes smaller than

$$\sqrt{k_p / \gamma_p}.$$

From the values of k_p and γ_p given for dipalmitoylphosphatidylcholine (DPPC) (25), this occurs close to 3 nm^{-1}. For smaller q, one would then have a constant protrusion contribution of ~0.025 nm^2 (based on the material constants for DPPC given in Brannigan and Brown (25)). This is consistent with the absence of q^{-2} protrusion behavior in our Fourier-based analysis. This increases q_{min} for the protrusion-dominated regime and it reduces the theoretical intensity to be comparable to the noise level in Figs. 4 and 5, suggesting that protrusions do not leave a significant or measurable footprint in the $S_u(q)$ spectra.

CONCLUSIONS

Our results show (see especially Figs. 4 and 5) that the simulated out-of-plane fluctuation spectrum $S_u(q)$ can be fit quite well to a model consisting only of undulations and the molecular density structure factor when $S_u(q)$ is calculated directly in Fourier space. In contrast, binning in real space introduces a filter that artifactually produces an $S_u(q)$ that can be fit, over the narrow available q range, by a q^{-2} term that traditionally has been considered as a signature of protrusions.

Of course, there are protrusions, as all simulation snapshots clearly show (see Fig. 1), and as is obvious from the width of the phosphate peaks in simulated electron density profiles along the z axis—both in small, flat-patch simulations and in large-scale simulations as reported in our next article (10). However, their footprint is so small in our $S_u(q)$ spectra that they are dominated by the two other contributions and thus have negligible effect on $S_u(q)$. This would be consistent with the traditional theory of protrusions only if the protrusions surface tension γ_p is larger than usually supposed. However, in the more recent theory (25), the presence of the constant k_p in Eq. 19 would further suppress the footprint of protrusions in $S_u(q)$ by pushing the signature q^{-2} behavior to larger q where it is even smaller; this is consistent with the simulation results we report.

SUPPORTING MATERIAL

Three sections, one figure, 35 equations, and five references are available at http://www.biophysj.org/biophysj/supplemental/S0006-3495(11)00320-1.

This work has been supported by the Swedish National Infrastructure for Computing with computer time at the High Performance Computing Center North, and has been funded by the Swedish Research Council with a grant to O.E. Additional computer resources were provided by the Minnesota Supercomputer Institute. J.F.N. acknowledges support from US National Institutes of Health grant No. GM 44976.

REFERENCES

1. Evans, E., and W. Rawicz. 1990. Entropy-driven tension and bending elasticity in condensed-fluid membranes. *Phys. Rev. Lett.* 64:2094–2097.
2. Evans, E. 1991. Entropy-driven tension in vesicle membranes and unbinding of adherent vesicles. *Langmuir.* 7:1900–1908.
3. König, S., W. Pfeiffer, …, E. E. Sackmann. 1992. Molecular dynamics of lipid bilayers studied by incoherent quasi-elastic neutron scattering. *J. Phys. II (France).* 2:1589–1615.
4. König, S., and E. Sackmann. 1996. Molecular and collective dynamics of lipid bilayers. *Curr. Opin. Colloid Interface Sci.* 1:78–82.
5. Rawicz, W., K. C. Olbrich, …, E. Evans. 2000. Effect of chain length and unsaturation on elasticity of lipid bilayers. *Biophys. J.* 79:328–339.
6. Pan, J., S. Tristram-Nagle, and J. F. Nagle. 2009. Effect of cholesterol on structural and mechanical properties of membranes depends on lipid chain saturation. *Phys. Rev. E.* 80:021931.
7. Helfrich, W. 1973. Elastic properties of lipid bilayers: theory and possible experiments. *Z. Naturforsch. C.* 28:693–703.
8. Faucon, J. F., M. D. Mitov, …, P. Bothorel. 1989. Bending elasticity and thermal fluctuations of lipid membranes. Theoretical and experimental requirements. *J. Phys. (France).* 50:2389–2414.
9. Marsh, D. 2006. Elastic curvature constants of lipid monolayers and bilayers. *Chem. Phys. Lipids.* 144:146–159.

10. Braun, A. R., E. G. Brandt, …, J. N. Sachs. 2011. Determination of electron density profiles and areas from simulations of undulating membranes. *Biophys. J.* 100:2112–2120.

11. Goetz, R., and R. Lipowsky. 1998. Computer simulations of bilayer membranes: self-assembly and interfacial tension. *J. Chem. Phys.* 108:7397–7409.

12. Lindahl, E., and O. Edholm. 2000. Mesoscopic undulations and thickness fluctuations in lipid bilayers from molecular dynamics simulations. *Biophys. J.* 79:426–433.

13. Edholm, O. 2008. Time and length scales in lipid bilayer simulations. *In* Computational Modeling of Membrane Bilayers. Current Topics in Membranes, Vol. 60, Chapt. 3. S. E. Feller, editor. Academic Press, London. 91–110.

14. Brandt, E. G., and O. Edholm. 2010. Stretched exponential dynamics in lipid bilayer simulations. *J. Chem. Phys.* 133:115101.

15. Goetz, R., G. Gompper, and R. Lipowsky. 1999. Mobility and elasticity of self-assembled membranes. *Phys. Rev. Lett.* 82:221–224.

16. Lipowsky, R., and S. Grotehans. 1993. Hydration vs. protrusion forces between lipid bilayers. *Europhys. Lett.* 23:599–604.

17. Lipowsky, R., and S. Grotehans. 1994. Renormalization of hydration forces by collective protrusion modes. *Biophys. Chem.* 49:27–37.

18. Vink, R. L. C., J. Horbach, and K. Binder. 2005. Capillary waves in a colloid-polymer interface. *J. Chem. Phys.* 122:134905.

19. Blokhuis, E. M. 2009. On the spectrum of fluctuations of a liquid surface: from the molecular scale to the macroscopic scale. *J. Chem. Phys.* 130:014706.

20. Stecki, J. 2004. Correlations in simulated model bilayers. *J. Chem. Phys.* 120:3508–3516.

21. Stecki, J. 2006. Size dependence, stability, and the transition to buckling in model reverse bilayers. *J. Chem. Phys.* 125:154902.

22. Stecki, J. 2010. Liquid bilayer and its simulation. *Adv. Chem. Phys.* 144:157–219.

23. Boek, E. S., J. T. Padding, …, W. J. Briels. 2005. Mechanical properties of surfactant bilayer membranes from atomistic and coarse-grained molecular dynamics simulations. *J. Phys. Chem. B.* 109:19851–19858.

24. May, E. R., A. Narang, and D. I. Kopelevich. 2007. Role of molecular tilt in thermal fluctuations of lipid membranes. *Phys. Rev. E.* 76:021913.

25. Brannigan, G., and F. L. H. Brown. 2006. A consistent model for thermal fluctuations and protein-induced deformations in lipid bilayers. *Biophys. J.* 90:1501–1520.

26. Berger, O., O. Edholm, and F. Jähnig. 1997. Molecular dynamics simulations of a fluid bilayer of dipalmitoylphosphatidylcholine at full hydration, constant pressure, and constant temperature. *Biophys. J.* 72: 2002–2013.

27. Berendsen, H. J. C., J. P. M. Postma, …, J. Hermans. 1981. Interaction models for water in relation to protein hydration. *In* Intermolecular Forces. B. Pullman, editor. Reidel, Dordrecht, The Netherlands. 331–342.

28. Lindahl, E., and O. Edholm. 2001. Molecular dynamics simulation of NMR relaxation rates and slow dynamics in lipid bilayers. *J. Chem. Phys.* 115:4938–4950.

29. Wohlert, J., and O. Edholm. 2006. Dynamics in atomistic simulations of phospholipid membranes: nuclear magnetic resonance relaxation rates and lateral diffusion. *J. Chem. Phys.* 125:204703–204710.

30. Marrink, S. J., A. H. de Vries, and A. E. Mark. 2003. Coarse grained model for semiquantitative lipid simulations. *J. Phys. Chem. B.* 108: 750–760.

31. Marrink, S. J., H. J. Risselada, …, A. H. de Vries. 2007. The MARTINI force field: coarse grained model for biomolecular simulations. *J. Phys. Chem. B.* 111:7812–7824.

32. Pearson, R. H., and I. Pascher. 1979. The molecular structure of lecithin dihydrate. *Nature.* 281:499–501.

33. Hess, B., C. Kutzner, …, E. Lindahl. 2008. GROMACS 4: algorithms for highly efficient, load-balanced, and scalable molecular simulation. *J. Chem. Theory Comput.* 4:435–447.

34. Kucerka, N., Y. Liu, …, J. F. Nagle. 2005. Structure of fully hydrated fluid phase DMPC and DLPC lipid bilayers using x-ray scattering from oriented multilamellar arrays and from unilamellar vesicles. *Biophys. J.* 88:2626–2637.

35. Hess, B. 2007. P-LINCS: a parallel linear constraint solver for molecular simulation. *J. Chem. Theory Comput.* 4:116–122.

36. Darden, T., D. York, and L. Pedersen. 1993. Particle mesh Ewald: an *n* log (*n*) method for Ewald sums in large systems. *J. Chem. Phys.* 98:10089–10092.

37. Essmann, U., L. Perera, …, L. G. Pedersen. 1995. A smooth particle mesh Ewald method. *J. Chem. Phys.* 103:8577–8593.

38. Nosé, S. 1984. A molecular dynamics method for simulations in the canonical ensemble. *Mol. Phys.* 52:255–268.

39. Hoover, W. G. 1985. Canonical dynamics: equilibrium phase-space distributions. *Phys. Rev. A.* 31:1695–1697.

40. Parrinello, M., and A. Rahman. 1981. Polymorphic transitions in single crystals: a new molecular dynamics method. *J. Appl. Phys.* 52:7182–7190.

41. Nosé, S., and M. L. Klein. 1983. Constant pressure molecular dynamics for molecular systems. *Mol. Phys.* 50:1055–1076.

42. Hansen, J. P., and I. R. McDonald. 2006. Theory of Simple Liquids, 3rd Ed. Academic Press, London.

43. Waheed, Q., and O. Edholm. 2009. Undulation contributions to the area compressibility in lipid bilayer simulations. *Biophys. J.* 97:2754–2760.

44. den Otter, W. K., and S. A. Shkulipa. 2007. Intermonolayer friction and surface shear viscosity of lipid bilayer membranes. *Biophys. J.* 93: 423–433.

45. Shkulipa, S. A. 2006. Computer simulations of lipid bilayer dynamics. PhD thesis. University of Twente, Enschede, The Netherlands.